Chemical Physics Letters 613 (2014) 64–69

Contents lists available at ScienceDirect

Chemical Physics Letters

journal homepage: www.elsevier.com/locate/cplett

Role of oxygen in Cu(1 1 0) surface restructuring in the vicinity of step edges

Liang Li [a], Na Cai [a], Wissam A. Saidi [b], Guangwen Zhou [a,*]

[a] Department of Mechanical Engineering & Multidisciplinary Program in Materials Science and Engineering, State University of New York, Binghamton, NY 13902, United States
[b] Department of Mechanical Engineering and Materials Science, University of Pittsburgh, Pittsburgh, PA 15261, United States

ARTICLE INFO

Article history:
Received 14 June 2014
In final form 19 August 2014
Available online 27 August 2014

ABSTRACT

Surface steps are typically assumed as a source of adatoms for oxygen-chemisorption induced surface reconstruction, but few microscopic observations have been made in the vicinity of steps on reconstructing surfaces. Using in situ scanning tunneling microscopy, we provide direct evidence that surface steps are the source of Cu adatoms for the Cu(1 1 0)—(2 × 1)-O restructuring. Using density functional theory, we show that the role of oxygen is to stabilize Cu adatoms detached from step edges via the barrier-less formation of Cu—O dimers on terraces. Incorporating this atomic process of capturing Cu adatoms into kinetic Monte Carlo simulations reproduces the experimentally observed (2 × 1)-O reconstruction.

1. Introduction

The exposure of a number of metallic surfaces including Cu, Ag and Ni to oxygen usually results in oxidation of the metal initiated by several progressive stages of phase transitions starting from oxygen chemisorption induced surface reconstruction to the nucleation and growth of surface oxide and then to the lateral spreading of the oxide. The process of oxygen-chemisorption induced restructuring of metal surfaces has received much attention. This interest stems from the critical role of chemisorbed oxygen in many technologically important processes including high-temperature corrosion, heterogeneous catalysis, surface passivation, and fuel reactions, in which oxygen chemisorption is a prerequisite to initiate the surface reactions [1].

Oxygen chemisorption on Cu(1 1 0) is a model system which has been studied extensively [2–17]. Molecular oxygen is known to dissociatively chemisorb on Cu(1 1 0) and results in a (2 × 1) "added-row" structure, in which the oxygen adatoms reside preferentially in the long-bridge (LB) sites of every other [0 0 1] rows of the Cu lattice [3–5,18–21]. The nucleation and growth of the (2 × 1) reconstruction have been assumed to occur via the following two steps [20–22]: (i) Cu atoms detach from step edges and diffuse out on the terraces, (ii) interaction of diffusing Cu adatoms with oxygen atoms impinging from the gas phase results in the anisotropic growth on the terraces of —Cu—O— added rows aligned parallel to the [0 0 1] direction of the Cu substrate. In this oxygen-chemisorption induced surface reconstructing process, surface steps are assumed to serve as a reservoir of Cu adatoms, and detachment of Cu atoms from the surface steps is considered as the rate-limiting step for the growth of —Cu—O— added rows [20–22]. It is noted that diffusion of oxygen can become a rate limiting factor for the oxide nucleation and growth following the oxygen chemisorption induced surface restructuring [23,24]. For the oxidation of other metallic surfaces such as Ru(0 0 0 1), it has been shown that oxide forms preferentially at step edges without a reconstruction of the metal surface, for which the supply of step-edge atoms is not the rate-limiting factor [25,26].

In spite of the wide acceptance of the aforementioned mechanism for the oxygen chemisorption induced Cu(1 1 0)—(2 × 1) reconstruction, surprisingly, the microscopic observations of surface steps as the source of Cu adatoms via step-edge detachment are still quite few. The edges of Cu(1 1 0) terraces were observed previously by scanning tunneling microscopy (STM) to become ragged upon oxygen exposure, which is attributed to the step-edge detachment of Cu adatoms for the growth of Cu—O added rows [20,21]. However, the previous study does not capture the nucleation and early-stage growth of (2 × 1) islands and thus does not provide clear evidence that Cu step-edge detachment is required for the oxygen chemisorption induced (2 × 1) restructuring. Particularly, the microscopic mechanism of how the chemisorbed oxygen influences the step-edge detachment of Cu atoms is not clearly established. In the work presented here, we utilize STM to visualize the dynamic

* Corresponding author.
E-mail addresses: gzhou@binghamton.edu, zhougw@yahoo.com (G. Zhou).

http://dx.doi.org/10.1016/j.cplett.2014.08.050
0009-2614/

evolution of a stepped Cu(1 1 0) surface during the initial stages of oxygen chemisorption. With use of in situ STM imaging to follow the nucleation and growth of —Cu—O— added rows with the coordinated retraction of surface steps of the Cu(1 1 0) substrate, we provide clear evidence that the oxygen chemisorption-induced (2×1) restructuring requires step-edge detachment of Cu adatoms. Using density-functional theory (DFT) and Kinetic Monte Carlo (KMC) simulations, we show that the major role of adsorbed oxygen is to capture diffusing Cu adatoms detached from step edges to form —Cu—O— compounds, thereby stabilizing detached Cu atoms on the terrace.

2. Experimental and computational methods

The STM experiments were performed by an ultrahigh vacuum (UHV) variable-temperature STM (Omicron VT-STM XA) with a base pressure of $\sim 1 \times 10^{-11}$ Torr. An electrochemically etched polycrystalline tungsten wire was used for the STM tip, which was flashed (1 kV and 2 mA) several times to evaporate adsorbates and native oxides. The Cu(1 1 0) single crystal is a 'top-hat' disk (1 mm thick and 8 mm in diameter), purchased from Princeton Scientific Corp., cut to within 0.1° to the (1 1 0) crystallographic orientation and polished to a mirror finish. The crystal was cleaned by repeated cycles of Ar^+ sputtering at room temperature (5×10^{-5} Torr of Ar^+, 1 μA cm^{-2}, 1.0 keV) followed by annealing at 600 °C for 10 min. Cleanliness of the Cu(1 1 0) surface was checked by STM imaging at room temperature prior to oxygen gas dosing. Oxygen gas (purity = 99.9999%) was introduced to the system through a variable-pressure leak valve at the oxygen pressure (pO_2) of 1×10^{-10} Torr. All the STM images were acquired at room temperature in constant-current mode with a bias on the sample.

The DFT calculations were performed using the Vienna ab initio simulation package (VASP) [27–30] with the PW91 generalized gradient approximation [31]. The projector augmented wave potentials [32] were chosen and the planewave cutoff energy was set to be 380 eV. The stepped Cu surfaces were modeled as periodic slabs consisting of two five-atom-row wide (1 1 0) terraces separated by a monatomic-height (1 0 0) step. The Cu slab contained 8 (1 1 0) layers with 168 atoms, and the bottom 3 layers were fixed throughout the structural relaxation. Successive slabs were separated by a vacuum region of 12 Å in the direction normal to (1 1 0) surface. The Brillouin zone was sampled using a $4 \times 2 \times 1$ Monkhorst–Pack mesh [33]. Electron smearing was carried out following the Methfessel–Paxton technique [34] with a Gaussian width of 0.2 eV. The structural optimization was terminated when all force components acting on the unconstrained atoms are less than 0.015 eV/Å. Various tests were performed to ensure that our computational framework such as **k**-grid convergence, vacuum size, and planewave cutoff yield reliable results [8,9]. We used the climbing image nudged elastic band (NEB) method [35] to determine the diffusion pathways and energy barriers. The surface adatoms hopping barriers used in the KMC simulations were obtained from our DFT calculations. The adsorption energy of oxygen is defined as

$$E_O^{\text{ads}} = \frac{1}{N_O}\left(E_{\text{O/Cu}}^{\text{tot}} - E_{\text{ref}} - \frac{N_O}{2}E_{O_2}\right)$$

where $E_{\text{O/Cu}}^{\text{tot}}$ is the total energy of the Cu—O system, E_{ref} is the energy of the structure before adsorbing oxygen, E_{O_2} is the energy of an isolated oxygen molecule, and N_O is the number of adsorbed oxygen adatoms.

3. Results and discussion

Fig. 1 shows a series of consecutive STM images of the Cu(1 1 0) surface with increasing oxygen exposure. As seen from Fig. 1(a), a screw dislocation intersects the Cu(1 1 0) surface, which results in the presence of a monoatomic-height (~1.30 Å) surface step oriented along the [0 0 1] direction. As a result, the surface exhibits two terraces separated by a monoatomic step. Before oxygen dosing, the surface step shows some thermal fluctuations but these do not induce any movements on the time scale (18 min) required

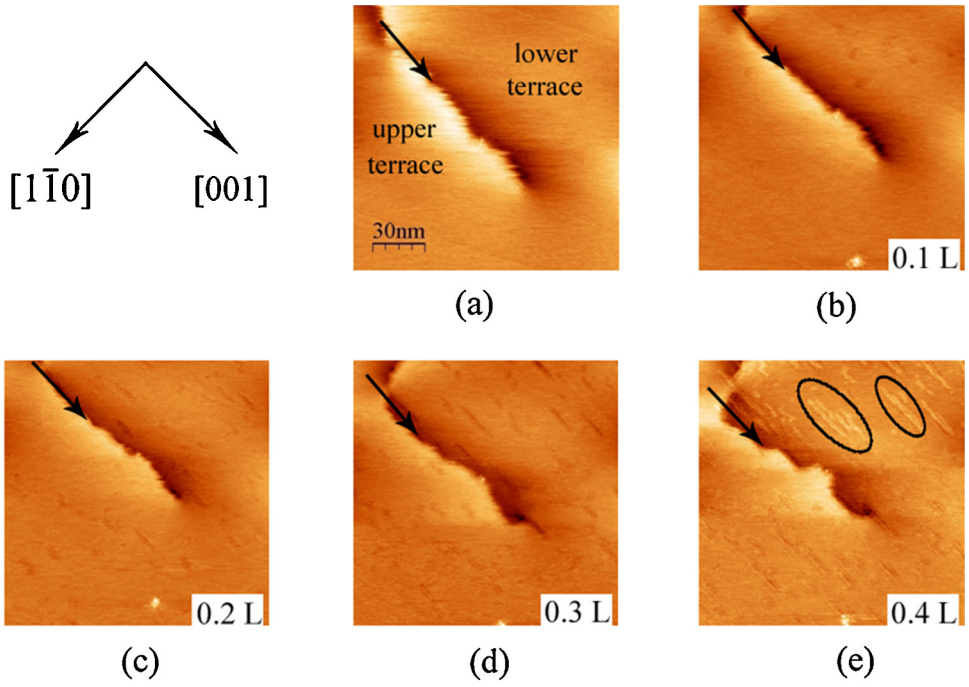

Figure 1. Consecutive topographic STM images of the Cu(1 1 0) surface showing the retraction of a surface step with oxygen exposure at $pO_2 = 1 \times 10^{-10}$ Torr and $T = 25$ °C: (a) the surface prior to oxygen exposure, (b) after 0.1 L oxygen exposure, (c) after 0.2 L oxygen exposure, (d) after 0.3 L oxygen exposure, (e) after 0.4 L oxygen exposure. The arrows shown on the upper-left corner mark the position of the step, which reveal that the step retracts by ~15 nm as the —Cu—O— added rows nucleate and grow on the terraces. The tunneling conditions for the STM imaging are $I_T = 0.5$–0.8 nA and $V_B = 1.5$–2 V.

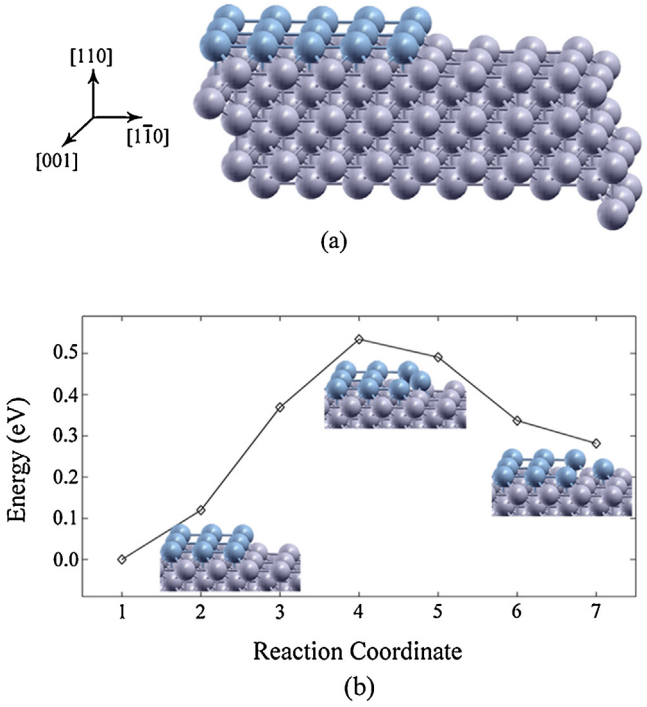

Figure 2. (a) The morphology of the DFT simulation cell of the clean stepped Cu(1 1 0) surface. (b) The minimum energy reaction path for the step-edge Cu detachment, where the initial, saddle-point, and final configurations are shown. Blue balls represent the Cu atoms at the upper terrace, and gray balls represent the underlying Cu atoms. (For interpretation of the references to color in this legend, the reader is referred to the web version of the Letter.)

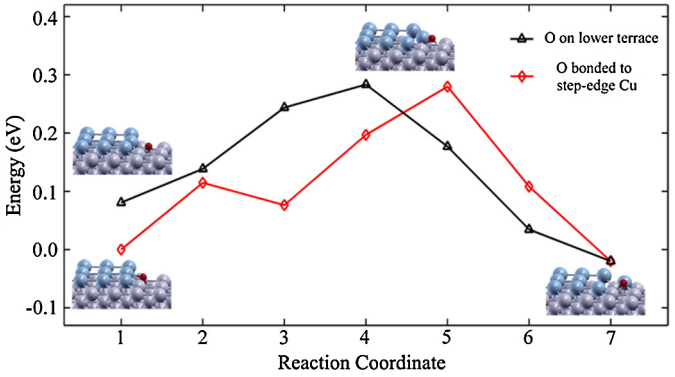

Figure 3. The minimum energy reaction path for the step-edge Cu detachment when an oxygen adatom is adsorbed directly onto step-edge Cu atoms and in the immediate vicinity of the step edge on the lower terrace, where the initial, saddle-point, and final configurations are shown. Blue, gray and red balls represent Cu atoms at the upper terrace, underlying Cu atoms and oxygen atoms, respectively. (For interpretation of the references to color in this legend, the reader is referred to the web version of the Letter.)

for a tunnel image, suggesting that the surface step is quite stable under the vacuum condition. Fig. 1(b–e) show the surface morphology evolution during the oxygen exposure at $p(O_2) = 1 \times 10^{-10}$ Torr in the time span of 68 min while performing tunneling images at room temperature. Consecutive images were taken at a time interval of 17 min. One can see that —Cu—O— rows nucleate and grow on the upper and lower terraces upon the oxygen exposure. With increasing oxygen coverage, these —Cu—O— rows form stripe-shaped domains of the (2×1)—O reconstruction that are aligned parallel to the surface step. Using the step edge location as a marker indicated by the arrows in Fig. 1(a–e), one can see that the surface step undergoes retraction from its original position with increasing oxygen coverage, which demonstrates rather nicely that Cu atoms are removed from the step edge to supply the growth of —Cu—O— added rows. It is noted that the initially straight step becomes corrugated. Meanwhile, the surface terraces remain flat during the oxygen exposure, indicating that the nucleation and growth of the —Cu—O— added rows under the low oxygen exposure does not involve extraction of Cu adatoms from terraces.

The in situ STM imaging of the early stages of the oxygen-chemisorption induced Cu(1 1 0)—(2×1) restructuring directly leads to a mechanistic understanding of the oxidation process. The step undergoes significant retraction and becomes faceted from the initially rather straight step to mutually perpendicular segments with the nucleation and growth of —Cu—O— chains on the terrace region. From the observed surface step retraction, it can be inferred that the individual Cu adatoms are highly mobile at room temperature and the atomic process of the oxygen chemisorption induced step-edge removal of Cu atoms cannot be directly resolved experimentally owing to the limited temporal resolution of STM imaging. We thus use DFT calculations to address how chemisorbed oxygen facilitates Cu step-edge detachment. The structure of the surface step in the simulation cell is shown in Fig. 2(a).

We first calculate the energy barrier for Cu atom detachment from the step edge for a clean surface and obtain the value of 0.53 eV. As shown in Fig. 2(b), the detached Cu atom resides in the LB site of the substrate in the saddle-point geometry, which is roughly the center of the transition path. Reversely, the barrier for a Cu atom to re-attach to the step edge is 0.25 eV (Fig. 2(b)). According to the transition state theory (TST) [36], the reaction rate can be calculated as $k = \nu_0 \exp(-E/K_B T)$, where ν_0 is the attempt frequency, E is the activation energy for detachment/re-attachment, K_B is Boltzmann constant and T is the temperature. For a temperature range of 300–450 K, it can be shown that the rate for re-attachment of Cu atoms to the step edge is 3–4 orders of magnitude higher than that of detachment by using the obtained activation energy barriers, 0.53 eV vs. 0.25 eV. Here for simplicity we assumed that the two processes have the same attempt frequency ν_0. This suggests that Cu atoms can easily re-attach to the step edge once it is dislodged. Therefore the stepped structure is stable against dissociation for the clean surface.

We then examine Cu detachment from the step edge in the presence of O. It has been shown that the [0 0 1] oriented —Cu—O— chains are very stable structures owing to the strong attractive interactions between Cu and O atoms [37]. We thus calculate the energy barrier for the formation of a [0 0 1] oriented Cu—O dimer, which serves as the nucleation seed for the (2×1)—O reconstruction. Oxygen atoms can be adsorbed at different locations in the vicinity of the step edge. Fig. 3 shows the energy profile of dimer formation process when an O atom is directly bonded to the step-edge Cu atoms, in which five intermediate images are added in between the initial and final configurations. Note that the system total energy drops marginally from Image 2 to Image 3 by 0.04 eV, which does not affect the calculation of overall reaction barrier. The adsorption energy of the O atom is calculated as −1.60 eV. The step-edge Cu atom bonded to the O atom detaches and diffuses to its adjacent hollow (H) site on the lower terrace to form a Cu—O dimer. The activation barrier for this oxygen-assisted Cu detachment is calculated as 0.28 eV, which is much smaller than the barrier for Cu detachment on the clean surface (0.53 eV). The detached Cu atom is at the LB site of the substrate in the saddle-point geometry, same as the case when O is absent. Cu re-attachment to the step is also likely to occur by overcoming an energy barrier of 0.30 eV.

O atoms can also be adsorbed on the lower terrace without being bonded to the step-edge Cu atoms. The most stable O adsorption site on flat Cu(1 1 0) terrace at low coverage is determined to be the pseudo threefold shifted-hollow (ShH) site, which is in agreement

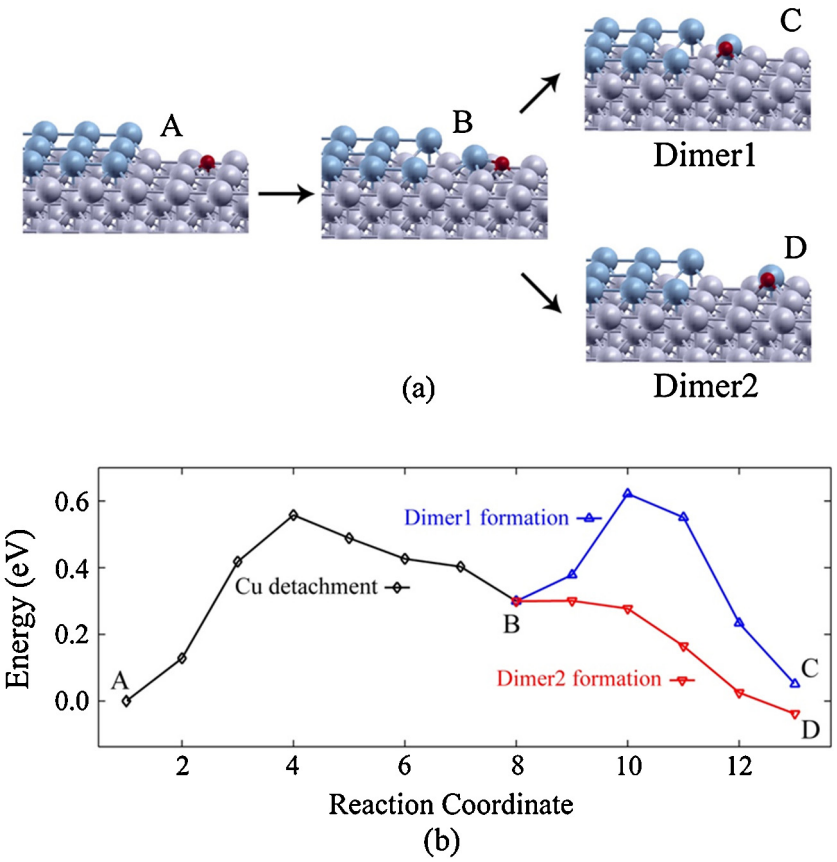

Figure 4. The detachment of step-edge Cu atom when an O atom is adsorbed on the lower terrace and the formation of the two possible Cu—O dimer structures. The initial position of the O atom is one [1 $\bar{1}$ 0] spacing far away from the step edge compared with that in Fig. 3. (a) Reaction A → B depicts the step-edge detachment of a Cu atom, and the paths B → C and B → D depict the formation of [0 0 1] oriented Cu—O dimers. (b) The corresponding NEB energy plot for the Cu detachment and dimer formation. Blue, gray and red balls represent Cu atoms at the upper terrace, underlying Cu atoms and oxygen atoms, respectively. (For interpretation of the references to color in this legend, the reader is referred to the web version of the Letter.)

with the previous theoretical studies [37,38]. We then investigate the effect of chemisorbed oxygen on the Cu step-edge detachment when O atom is on the lower terrace. An O adatom is placed at the ShH site in the immediate vicinity of the step edge as shown in Fig. 3, and the adsorption energy is calculated as −1.51 eV. The dimer formation process shown in Fig. 3 strikingly resembles the case where O is bonded to Cu atoms belonging to step edge: the energy barrier for Cu detachment is 0.20 eV, whereas the barrier for the reverse process is 0.30 eV, and the detached Cu atom also resides the LB site of the substrate in the saddle-point geometry. These calculations indicate that Cu detachment becomes much easier when the O adatom is adsorbed in the immediate vicinity of the step edge, either directly bonded to the step-edge Cu atoms or on the lower terrace adjacent to the step edge, however, in both cases the detached Cu atoms are highly possible to re-attach to the step edge by breaking the Cu—O bonds due to the low activation energy.

Considering that O adatoms can be adsorbed at various ShH sites on the lower terraces, we then place the adsorbed oxygen adatom at an ShH site which is one more [1 $\bar{1}$ 0] spacing away from the step edge, and let the step-edge Cu atom detach and diffuse to its adjacent H site, as illustrated by configurations A and B in Fig. 4(a). The O adsorption energy of configuration A is −1.67 eV, which is marginally lower than the initial configurations shown in Fig. 3, suggesting that the ShH site in configuration A is slightly more favorable for O adsorption. The result of the NEB calculation of the Cu detachment process is shown in Fig. 4(b). The energy barrier for the Cu step-edge detachment (process A–B) is calculated to be 0.56 eV. Compared with the energy barrier of 0.53 eV for Cu detachment from the step edge on a clean surface, it is quite counterintuitive that the presence of chemisorbed O adjacent to the surface step does not make the Cu step-edge detachment easier, but rather renders it slightly more difficult to break the Cu—Cu bonds at the step edge. Furthermore, by comparing the total energies of configurations A and B, it is found that the total system energy is increased by about 0.30 eV after the Cu atom is detached from the step edge. This suggests that configuration B is not energetically as favorable as configuration A.

There are two possible dimer structures resulting from structure B, which are depicted as structures C (same as the final configuration in Fig. 3) and D shown in Fig. 4(a). The positions of Dimer1 and Dimer2 differ by one [1 $\bar{1}$ 0] spacing. The obtained energy barriers for the formation of the two dimer structures are shown in Fig. 4(b). The formation of Dimer1 can be viewed as oxygen moving toward the step edge, which needs to overcome an energy barrier of 0.32 eV, while the formation of Dimer2 is essentially caused by the diffusion of the detached Cu atom away from the step edge, and the system energy keeps decreasing along the Dimer2 formation path. This suggests that configuration B is not a stable structure, and evolves naturally to Dimer2 (configuration D) without experiencing any energy barriers. In addition, the reaction barrier for the transition from configuration D to A is 0.60 eV, which suggests that once Dimer2 is formed, it becomes unlikely for the detached Cu atom to re-attach to the step edge. Therefore, the process A → D is the favored process for the step-edge detachment of Cu atoms. DFT calculations indicate that the effect of O adatom in this case is not to make the Cu detachment from the step edge easier compared to the case in which oxygen is adsorbed adjacent to the step edge. Instead, the adsorbed O captures free Cu adatoms to form Cu—O

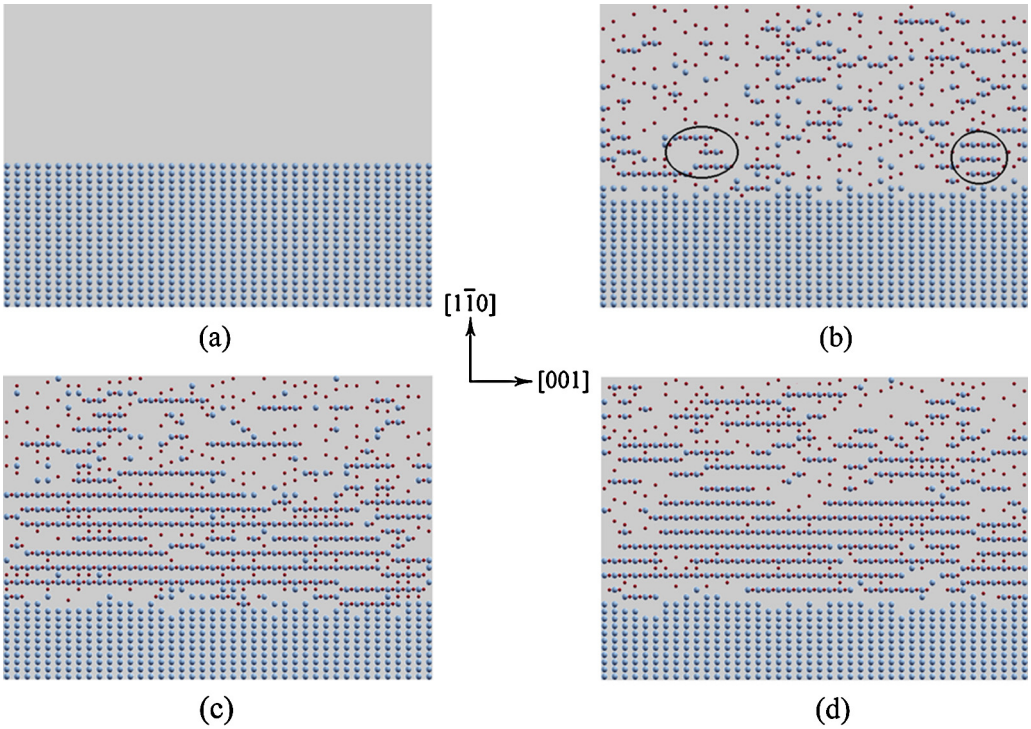

Figure 5. Dynamic morphological evolution of the stepped Cu(1 1 0) surface in KMC simulations. (a) Morphology of stepped surface, with no oxygen introduced into the system. (b) Morphology of the surface covered by 0.35 monolayer (ML) oxygen, with the oxygen deposition rate of 0.01 ML per hour Morphology of the surface covered by 0.5 ML oxygen, with the oxygen deposition rate of 0.01 ML per hour. (d) Morphology of the surface covered by 0.5 ML oxygen, with the oxygen deposition rate of 0.03 ML per hour. Blue balls represent Cu atoms and smaller red balls represent oxygen adatoms. (For interpretation of the references to color in this legend, the reader is referred to the web version of the Letter.)

dimers parallel to the [0 0 1] direction, which not only brings down the system energy without the need of overcoming large energy barriers, but also reduces the concentration of Cu adatoms on the terrace from the equilibrium concentration, thereby resulting in a net flux of Cu adatoms from the step edge.

With the identified atomic processes as illustrated in Fig. 4 and the energy barriers obtained from the DFT calculations, we then use KMC to simulate the nucleation and growth of —Cu—O— added rows, in which the Cu step-edge detachment process is incorporated by using the reaction barriers listed before. The hopping rate of an adatom is determined by the equation $k = \nu_0 \exp(-E/K_B T)$, where E is the activation energy for each hopping event, which is obtained by DFT calculations. We choose a universal attempt frequency $\nu_0 = 10^{12}\ s^{-1}$ for each hopping since this value is used in most of the KMC simulations on the Cu system [39–41]. As shown in Fig. 5(a), the simulation starts with a 2D grid partially covered by Cu atoms to mimic a stepped Cu(1 1 0) surface with a monatomic-height step, which serves as the source of Cu adatoms via step-edge detachment. Periodic boundary condition is applied along the [0 0 1] direction, and adatoms are confined on the terrace so that they would not go beyond the 2D grid along the [1 $\bar{1}$ 0] direction. Tests with various sizes of simulation grids confirm that the nonperiodicity of the grid does not affect the simulated surface morphology. The simulations are carried out on an 85×85 grid, and the upper terrace is constructed by 20 Cu [001] rows, where the Cu atoms are mapped on the grid points whose row and column numbers are both even (shown in Fig. 5(a)). It typically takes 10^4 steps for the system to reach a stabilized morphology, where one KMC step is defined as the interval within which the hopping events of all the Cu and O adatoms are considered once. Oxygen adatoms are introduced onto the lower terrace randomly at a constant rate for each simulation, and the effect of oxygen desorption is not included. For simplicity, no oxygen adatoms are deposited onto the upper terrace. The simulation time is advanced after each adatom movement, as implemented in traditional KMC scheme [42,43]. It should be noted that discrepancies between the KMC simulation time and real experimental time are often observed [44], and the simulation time of 10^4 KMC steps for the 2D grid used in this work is typically on the order of 10^6 s, which far exceeds the experimental time of about 4000 s.

Fig. 5(b) and (c) shows the dynamic evolution of the stepped Cu(1 1 0) surface at a deposition rate of 0.01 ML per hour. As shown in the circled regions in Fig. 5(b), some bundled short —Cu—O— chains can be observed when the oxygen coverage reaches 0.35 ML on the lower terrace, which is consistent with the experimental results that —Cu—O— chains tend to form adjacent to each other [20,21]. The stable surface structure at a higher oxygen coverage of 0.5 ML is presented in Fig. 5(c), in which more —Cu—O— chains are formed at the lower terrace, and generally the lengths of the chains are longer than those in Fig. 5(b). Various deposition rates are tested to study the effect of oxygen flux rate on the surface morphology evolution. It is found that a higher oxygen deposition rate does not lead to appreciable changes in the stable surface structure. As shown in Fig. 5(d), when oxygen adatoms are introduced at the rate of 0.03 ML per hour, the overall surface morphology at the 0.5 ML of oxygen coverage on the lower terrace is similar to that obtained with the slower oxygen deposition rate (Fig. 5(c)). It can be noted from the step edge profiles shown in Fig. 5(c) and (d) that despite the different oxygen deposition rates, the retractions of the original Cu steps are almost the same. A quantitative analysis shows that the amounts of detached Cu atoms for the deposition rates of 0.01 and 0.03 ML per hour are 48.1% and 46.8%, respectively. This indicates that the rate of Cu removal from the step edge and the growth of Cu—O— chains are independent of O impingement rate, which corroborates well with the experimental results [22].

It is expected that with the abundant supply of Cu and O adatoms and sufficient reaction time, the ideal equilibrium surface structure with 0.5 ml oxygen coverage should be a perfect (2×1)—O reconstructed surface [45]. As shown in Fig. 5(c) and (d), the vicinity of the step edge is covered by long, continuous —Cu—O— added rows. However, on the surface area relatively far away from the step, Cu and O atoms tend to form shorter —Cu—O— segments. It is worth noting that the diffusion of Cu—O dimers is also considered in our KMC simulations. Our NEB calculations show that the energy barrier for the diffusion of a Cu—O dimer along the [0 0 1] direction of the Cu(1 1 0) surface is as large as 1.75 eV, whereas the barrier for the diffusion along $[1\ \bar{1}\ 0]$ is 0.64 eV. The diffusion processes with reaction barriers well over 1 eV are typically ignored [46]. Therefore, the Cu—O dimer diffusion along the $[1\ \bar{1}\ 0]$ direction is included in our KMC simulation while the dimer diffusion along the [0 0 1] direction is ignored. We have also calculated the energy barriers for the diffusion of a Cu—O—Cu trimer along the [0 0 1] and $[1\ \bar{1}\ 0]$ directions, which have the values of 2.91 eV and 1.20 eV, respectively. The trimer diffusion is therefore ignored in our KMC model due to the large barriers.

A close examination of the KMC results as shown in Fig. 5 indicates that almost all Cu adatoms are bonded to at least one O adatom, while there are still a large number of un-bonded O adatoms on the terrace. Therefore, the discontinuity of —Cu—O— chains across the entire terrace is caused by the limited supply of Cu adatoms. This is because the step is the only source of Cu adatoms and the formation of —Cu—O— chains in the vicinity of the step edge can block detached Cu adatoms and Cu—O dimers from diffusing out, which in turn stabilizes the surface step from the step-edge detachment. Since the Cu supply to the terrace regions away from the step edge cannot keep up with the influx of adsorbing O, there are a large number of discrete and short —Cu—O— segments as well as un-bonded O atoms on these regions as seen in Fig. 5(c) and (d). In reality, however, the flat terrace may become another source of Cu adatoms when the incoming O_2 flux far outweighs the amount of Cu adatoms on the terraces and those from the step edges. Cu atoms can then be expelled from the terrace and form —Cu—O— chains on these terrace regions away from the step edge, which results in the formation of one-layer deep depressions on the terrace. Such a process of forming Cu adatoms from the terrace was observed experimentally [45,47] but is beyond the reach of our KMC simulations.

4. Conclusions

The oxygen chemisorption induced reconstruction of a stepped Cu(1 1 0) surface is studied using STM in conjunction of DFT and KMC. It is shown by in situ STM observation that surface steps are the source of Cu adatoms for the (2×1) added-row restructuring. Using first-principle total energy calculations, we clarify that the O adatoms adsorbed in the immediate vicinity of the surface step can destabilize step-edge atoms, but the step edge detachment of Cu atoms is more favored by oxygen adsorption away from the step edge, for which the detached Cu atoms are bonded more strongly with adsorbed O to form —Cu—O— added rows. Incorporation of the identified atomic processes into KMC simulations reproduces the experimentally observed nucleation and growth of the Cu(1 1 0) (2×1)—O added rows. Our KMC simulations also demonstrate that the variations in the oxygen impingement rate have no appreciable change in the amount of detached Cu adatoms, suggesting that Cu step-edge detachment is the rate-limiting step in controlling the growth of —Cu—O— rows.

Acknowledgments

This work was supported by the U.S. Department of Energy, Office of Basic Energy Sciences, Division of Materials Sciences and Engineering under Award No. DE-FG02-09ER46600. W. Saidi acknowledges the support of NSF under Grant No. DMR-1410055. The authors thank N.P. Guisinger for help with the STM experiments. Use of the Center for Nanoscale Materials was supported by the U.S. Department of Energy, Office of Science, Office of Basic Energy Sciences, under Contract No. DE-AC02-06CH11357. This work used the Extreme Science and Engineering Discovery Environment (XSEDE), which is supported by National Science Foundation Grant number OCI-1053575.

References

[1] N. Reinecke, S. Reiter, S. Vetter, E. Taglauer, Appl. Phys. A: Mater. Sci. Process. 75 (2002) 1.
[2] S.R. Parkin, H.C. Zeng, M.Y. Zhou, K.A.R. Mitchell, Phys. Rev. B 41 (1990) 5432.
[3] U. Döbler, K. Baberschke, J. Haase, A. Puschmann, Phys. Rev. Lett. 52 (1984) 1437.
[4] H. Dürr, T. Fauster, R. Schneider, Surf. Sci. 244 (1991) 237.
[5] K. Bobrov, L. Guillemot, Phys. Rev. B 78 (2008) 121408.
[6] C. Poulain, F. Wiame, V. Maurice, P. Marcus, Surf. Sci. 606 (2012) L26.
[7] P. Singnurkar, I. Bako, H.P. Koch, E. Demirci, A. Winkler, R. Schennach, J. Phys. Chem. C 112 (2008) 14034.
[8] G.W. Zhou, L.L. Luo, L. Li, J. Ciston, E. Stach, J.C. Yang, Phys. Rev. Lett. 109 (2012) 235502.
[9] L. Li, G.W. Zhou, Surf. Sci. 615 (2013) 57.
[10] F.M. Chua, Y. Kuk, P.J. Silverman, Phys. Rev. Lett. 63 (1989) 386.
[11] S.Y. Liem, J.H.R. Clarke, G. Kresse, Surf. Sci. 459 (2000) 104.
[12] S.L. Silva, R.M. Lemor, F.M. Leibsle, Surf. Sci. 421 (1999) 135.
[13] Y. Uehara, T. Matsumoto, S. Ushioda, Phys. Rev. B 66 (2002) 075413.
[14] F. Frechard, R.A. van Santen, Surf. Sci. 407 (1998) 200.
[15] R.A. DiDio, D.M. Zehner, E.W. Plummer, J. Vac. Sci. Technol. A 2 (1984) 852.
[16] G. Dorenbos, M. Breeman, D.O. Boerma, Phys. Rev. B 47 (1993) 1580.
[17] E. Demirci, J. Stettner, M. Kratzer, R. Schennach, A. Winkler, J. Chem. Phys. 126 (2007) 164710.
[18] R.P.N. Bronckers, A.G.J. de Wit, Surf. Sci. 112 (1981) 133.
[19] R. Feidenhans'l, I. Stensgaard, Surf. Sci. 133 (1983) 453.
[20] D.J. Coulman, J. Wintterlin, R.J. Behm, G. Ertl, Phys. Rev. Lett. 64 (1990) 1761.
[21] F. Jensen, F. Besenbacher, E. Lægsgaard, I. Stensgaard, Phys. Rev. B 41 (1990) 10233.
[22] F. Besenbacher, F.B. Norskov, Prog. Surf. Sci. 44 (1993) 5.
[23] J.C. Yang, M. Yeadon, B. Kolasa, J.M. Gibson, Appl. Phys. Lett. 70 (1997) 3522.
[24] G.W. Zhou, J.C. Yang, Surf. Sci. 531 (2003) 359.
[25] B. Herd, M. Knapp, H. Over, J. Phys. Chem. C 116 (2012) 24649.
[26] B. Herd, J.C. Goritzka, H. Over, J. Phys. Chem. C 117 (2013) 15148.
[27] G. Kresse, J. Hafner, Phys. Rev. B 47 (1993) 558.
[28] G. Kresse, J. Hafner, Phys. Rev. B 49 (1994) 14251.
[29] G. Kresse, J. Furthmüller, Comput. Mater. Sci. 6 (1996) 15.
[30] G. Kresse, J. Furthmüller, Phys. Rev. B 54 (1996) 11169.
[31] J.P. Perdew, et al., Phys. Rev. B 46 (1992) 6671.
[32] G. Kresse, D. Joubert, Phys. Rev. B 59 (1999) 1758.
[33] H.J. Monkhorst, J.D. Pack, Phys. Rev. B 13 (1976) 5188.
[34] M. Methfessel, A. Paxton, Phys. Rev. B 40 (1989) 3616.
[35] G. Henkelman, B.P. Uberuaga, H. Jonsson, J. Chem. Phys. 113 (2000) 9901.
[36] K.J. Laidler, M.C. King, J. Phys. Chem. 87 (1983) 2657.
[37] S.Y. Liem, G. Kresse, J.H.R. Clarke, Surf. Sci. 415 (1998) 194.
[38] X. Duan, O. Warschkow, A. Soon, B. Delley, C. Stampfl, Phys. Rev. B 81 (2010) 075430.
[39] C. Mottet, Surf. Sci. 417 (1998) 220.
[40] H. Mehl, O. Biham, I. Furman, Phys. Rev. B 60 (1999) 2106.
[41] C. Sendner, S. Sakong, A. Groß, Surf. Sci. 600 (2006) 3258.
[42] A.F. Voter, in: K.E. Sickafus, E.A. Kotomin, B.P. Uberuaga (Eds.), Radiation Effects in Solids, Springer, Dordrecht, 2007, p. 1.
[43] A. Farkas, F. Hess, H. Over, J. Phys. Chem. C 2 (2012) 581.
[44] K.A. Fichthorn, W.H. Weinberg, J. Chem. Phys. 95 (1991) 1090.
[45] Q. Liu, L. Li, N. Cai, W.A. Saidi, G. Zhou, Surf. Sci. 627 (2014) 75.
[46] W. Zhu, F. Buatier de Mongeot, U. Valbusa, E.G. Wang, Z. Zhang, Phys. Rev. Lett. 92 (2004) 106102.
[47] L. Sun, M. Hohage, R. Denk, P. Zeppenfeld, Phys. Rev. B 76 (2007) 245412.